JOURNAL OF MATERIALS SCIENCE 32 (1997) 5069–5083

Reciprocating sliding friction and contact stress of some thermoplastics against steel

H. S. BENABDALLAH
Department of Mechanical Engineering, Royal Military College of Canada, P.O. Box 17000, Kingston, Ontario, Canada K7K 7B4

This study considers the sliding friction in reciprocating motion, plane on plane and dry contact between very smooth surface of a steel slider and three engineering thermoplastics: ultrahigh-molecular weight polyethylene, polyoxymethylene and PA 66. Dynamic coefficients of friction were accurately measured at ranges of apparent contact pressure varying between 25 and 800 kPa and sliding speed between 0.01 and 0.1 m s^{-1}, using plastic samples whose surface roughness was fully characterized. The frictional behaviours in reciprocating motion were found to be equivalent to those reported by previous workers who have tested similar materials in continuous motion. These results were used in the evaluation of non-Hertzian elastic contact stresses considering a simplified model of cylindrical tips of asperities of plastic materials making contact with a polished and hard semi-infinite plane. Fatigue failure analysis was conducted and the combination of the Marin equation and the Soderberg fatigue failure criterion used to evaluate the factor of safety. The results of this analysis were summarized graphically in the form of load–frequency capabilities that represent the onset of excessive fatigue wear for each plastic material. Scanning electron microscopy observations of worn plastic samples enabled the illustration of the mechanism of formation of wear particles in the case of the present tribological system. The results of the qualitative evaluation of the amount of wear showed the importance of the decrease in normal load in order to increase the factor of safety, despite the increase in the coefficient of friction so induced for most thermoplastics.

1. Introduction

A considerable number of papers dealing with tribological behaviours of plastic materials have been published, and in most cases the experimental results on the friction and wear of these materials were reported. Particular attention was devoted to engineering thermoplastics because of their suitability for fabricating machine elements that support or transmit loads. During these situations the materials are subjected to contact stresses. The literature review demonstrates that polyethylenes, especially ultrahigh-molecular-weight polyethylene (UHMWPE), polyamides and polyacetals (virgin or containing fibres, fillers or solid lubricants), were extensively investigated in order to understand the phenomena arising when they are involved in static or dynamic contact with either the same material or a material having different properties. Their low surface energies, varying between 20×10^{-3} and 40×10^{-3} J m^{-2} at 20 °C [1], and strong dependence of their mechanical properties on time and temperature were found to have a major impact on the phenomenology of friction and wear of these materials, which distinguish them from conventional metallic materials such as steel and aluminium.

Despite considerable interest and effort, some fundamental related aspects remain difficult to explain and there is still a need for reliable data or practical and simple models that could be used to predict contact parameters needed during the design of technical applications. The non-linear relationship found between the frictional force and normal load was one of the main aspects of interest, and it is now well recognized that the coefficient of friction of these materials is strongly affected by the operating variables such as load and speed but also by the topography of contacting surfaces and environment.

Tribosystems consisting of plastic materials in dry sliding against harder materials such as steel have proved to be favourable for the formation of interfacial films, commonly called a third body, between the slider and the counterface. It is now well established that advantageous friction operations (if a low coefficient of friction is required) depend on the formation and transfer of these films which lead to relatively lower wear. However, although interest has been dedicated to this fundamental aspect, details of the processes of film formation are still not very well defined. Obviously the initial roughness of the metallic counterface may play an important role in such transfer, and an optimal roughness was suggested by some researchers, among them Dawson *et al.* [2] and Tanaka and Nagai [3]. Generally, it was observed

0022–2461

that a roughness of about 0.1 μm root mean square (RMS) gives minimum wear.

The review of the literature revealed also that a pin-on-disc apparatus or a similar set-up was most commonly used in experimental studies. These tribometers were preferred because of their simplicity even though it was recognized that they do not reproduce adequately many of the contact situations found in practical applications and are very much subjected to vibrations. It appears that only a very limited number of studies has been carried out on reciprocating motion despite its relatively large application. During this type of motion, sudden transitions take place at the beginning of each stroke, owing to the change in friction regime from static to dynamic. These conditions may introduce friction and wear mechanisms which would not normally be present during unidirectional sliding, where this type of transition takes place only at start up. Tolstoi [4] has investigated the relative motion between bodies making contact and concluded that transition from static to sliding friction develops during these situations.

On the basis of the observations mentioned above, and in an attempt to contribute further to this field, the global objective of this study is to illustrate the friction and wear performance of three commercially available engineering thermoplastics, namely UHMWPE, acetal (also known as polyoxymethylene (POM)) and nylon (PA 66), when tested in plane-on-plane contact configuration under dry conditions against a polished steel counterface in reciprocating motion. A fairly large nominal area of contact, more representative of actual situations, is considered. Tribological behaviours such as effects of normal load and sliding speed on the contact stresses induced in these plastic materials are investigated. An attempt is also made to investigate and analyse the fatigue phenomena generated, at the tips of the asperities of these materials during this type of friction; particular attention is given to conditions when fatigue failure may occur leading to excessive fatigue wear.

2. Experimental procedure and materials

The rig used in this study was pressented and described in full in a previous paper [5]. Without going into details in repeating its description, we should, however, point out that stationary blocks of plastic materials, called hereafter samples, are pressed against a steel slider moving in a reciprocating motion, generated by a universal hydraulic testing machine. Three importance features of this device should be mentioned.

1. The frictional force is measured by a load cell whose measurement axis lies exactly on the plane of contact between the two bodies (sample and slider).
2. The sample is permitted to have two degrees of freedom, so that perfect plane on plane contact is ensured between the two friction components.
3. Care was taken in the design stage in order to prevent a self-energizing effect in the system, thus ensuring that the normal load is not perturbed by the creation of the frictional force during sliding.

Three commercially available engineering thermoplastics normally used in sliding applications were investigated. Samples in a form of blocks were cut from extruded sheets of UHMWPE (Hercules 1900) supplied by Solidur, PA 66 (Zytel 101) and POM (Delrin 500) both supplied by DuPont. These plastic materials were characterized and the values of properties relevant to this study, as well as the testing methods used, are listed in Table I. These values represent an average of results of five consecutive tests which in all cases have been relatively low standard deviations.

Care was taken in order to ensure that the direction of extrusion coincided always with the direction of sliding, to avoid the introduction of an additional variable into the tribological system.

The contacting surface of these samples, having an apparent area of contact of 20 mm × 10 mm was machined using a milling machine. The counterface was made of cold-rolled steel AISI 4340 (Rockwell C hardness, 58 HRC) and consisted of a slider having an overall area of 110 mm × 15 mm. After machining, the samples were carefully cleaned from any wear debris. Furthermore, they were subjected to an annealing treatment in order to relieve the induced residual stresses. Finally, prior to testing, they were placed in a desiccator to control and normalize moisture, which is more critical in the case of PA 66.

The topographical parameters of the contacting surfaces pertinent to this study were measured by a surface roughness tester (Surftest 301 series 178) which gave the centre-line average (CLA) and RMS values as well as the number of profile peaks per unit length.

TABLE I Properties of the plastic materials

Property	Units	Testing method	Value for following materials		
			UHMWPE	POM	PA 66
Hardness	MPa	Kenton microhardness, 3 N load for 10 s	73	204	231
Modulus of elasticity	GPa	ASTM D-638	1.2	2.5	2.2
Poisson's ratio			0.46	0.35	0.34
Yield strength	MPa	ASTM D-638 (0.2% offset)	25	65	77
Tensile strength	MPa	ASTM D-638 (at yield)	28	70	83
Shear strength	MPa	ASTM D-732	20	70	62
Degree of crystallinity	%	DSC	73	81	94
Glass transition temperature	°C	DMTA	− 95	− 180	65
Melting temperature	°C	DSC	125	180	255

TABLE II Topographical parameters of the contacting surfaces

	Total number of peaks	CLA (μm)	RMS (μm)	Average deviation of peak height (μm)	Radius of tips of asperities (μm)
UHMWPE sample	376	0.8	0.97	0.52	9.5
POM sample	380	0.78	0.89	0.34	8.6
PA 66 sample	378	0.92	1.3	0.31	9
Steel slider (polished)	(Smooth)	0.16	0.19	—	—

In order to characterize the surface texture of the plastic materials further, appropriate signals emitted by this apparatus were fed into a computer through a data acquisition board. The average deviation of peak height was determined from usual statistical analysis, and the radius of asperity tips calculated using the following equation [6]:

$$r = \frac{\delta_v}{\delta_h^2}\frac{d^2}{8h} \tag{1}$$

where δ_v and δ_h are the vertical and horizontal magnifications, respectively, and d is the width of the asperity calculated at a distance $h = 0.3$ CLA from the crest of the peak. The values obtained for these topographical parameters are reported in Table II and represent the average based on data obtained from three traces of the stylus; two near the edges and the third along the middle line of the surface of the sample, in the same direction as the sliding motion. Three samples of each material were characterized in order to examine the reproducibility of the results. The digitized profile showed a very-well-defined geometry of asperities, making the analysis easier to conduct and at the same time decreasing uncertainties. The surface finish was obtained at very low feed, of the milling machine.

The CLA and RMS values characterizing the polished steel counterface were also included in Table II.

We should point out that it was reported by Benabdallah and Chalifoux [7] that plastic deformation occurs at regions where there is contact with the stylus of the profilometer during the surface characterization of plastic materials. No attempt was made here to introduce any correction to the reported data, but the samples that served in this operation were not used further in friction testing.

3. Contact stresses

As pointed out above, the very-well-defined profile of asperities permitted the contact problem to be simplified by reducing it to the model shown in Fig. 1 in which an idealized rough surface of the sample (plastic material) having asperities of equal height and cylindrical tips transverse to the sliding direction makes contact with a rigid (steel) and perfectly plane smooth semi-infinite surface.

It is important to note that the following analysis does not take into account the generation of heat during friction which would certainly affect the fatigue process of the asperities. Also, creep is not considered and it is assumed that adhesion occurs between the tips of the asperities and the sliding surface.

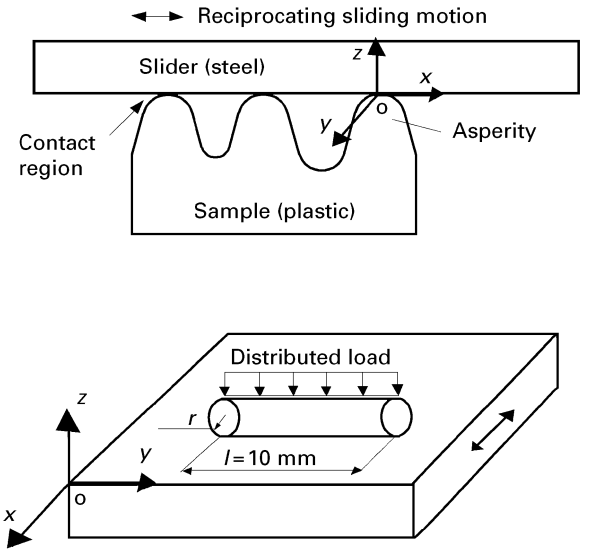

Figure 1 Model contact simulation for non-Hertzian elastic stress analysis.

Following the above-mentioned conditions on which the present study was based, the non-Hertzian elastic stresses that develop in the contact region, with respect to the axis system shown in Fig. 1, can be calculated using the following equations [8]:

$$\sigma_z = -\frac{b}{\pi\Delta}\left[z(b\varphi_1 - x\varphi_2) + \mu z^2\varphi_2\right] \tag{2}$$

$$\sigma_y = \nu(\sigma_x + \sigma_z) \tag{3}$$

$$\sigma_x = -\frac{b}{\pi\Delta}\left[z\left(\frac{b^2 + 2z^2 + 2x^2}{b}\varphi_1 - \frac{2\pi}{b} - 3x\varphi_2\right) + \mu(2x^2 - 2b^2 - 3z^2)\varphi_2 + \frac{2\pi x}{b} + 2(b^2 - x^2 - z^2)\frac{x}{b}\varphi_1\right] \tag{4}$$

$$\tau_{xz} = \frac{b}{\pi\Delta}\left[z^2\varphi_2 + \mu\left((2x^2 + b^2 + 2z^2)\frac{z}{b}\varphi_1 - \frac{2\pi z}{b} - 3xz\varphi_2\right)\right] \tag{5}$$

where

$$\varphi_1 = \frac{\pi(M+N)}{MN(2MN + 2x^2 + 2z^2 - 2x^2 + 2z^2 - 2b^2)^{1/2}} \tag{6}$$

$$\varphi_2 = \frac{\pi(M-N)}{MN(2MN + 2x^2 + 2z^2 - 2x^2 + 2z^2 - 2b^2)^{1/2}} \tag{7}$$

$$M = [(b+x)^2 + z^2]^{1/2} \tag{8}$$

$$N = [(b-x)^2 + z^2]^{1/2} \tag{9}$$

$$b = \left(\frac{2w\Delta}{\pi}\right)^{1/2} \tag{10}$$

$$\Delta = 2r\left(\frac{1-\nu_1^2}{E_1} + \frac{1-\nu_2^2}{E_2}\right) \tag{11}$$

in which w is the distributed load acting on one asperity ($w = F_n/l\eta$) calculated from the applied normal load F_n, the sample width, $l = 10$ mm, and the number of asperities, η, given in Table II. The value of the radius of the tip of the asperities, r, as shown in Fig. 1 is also given in Table II.

Furthermore, the presence of the shear stress in the x–z plane gives two principal stresses which are called here σ_1 and σ_2 and are determined from Mohr's circle. By assuming a state of normal strain, the third stress, σ_3, becomes equivalent to σ_y. The maximum shear stress, τ_{max}, is the largest magnitude of the three extreme values of shear stresses also determined from Mohr's circles as the radius of each circle. The von Mises stress given by the following equation, which is a function of these principal stresses, is used here to verify whether inelastic action takes place at critical points located in contact regions:

$$S_{vM} = \frac{1}{2^{1/2}}[(\sigma_1 - \sigma_2)^2 + (\sigma_2 - \sigma_3)^2 + (\sigma_3 - \sigma_1)^2]^{1/2} \tag{12}$$

It is clear that, in the situation of the present study, the fatigue phenomenon of the asperities is more pronounced owing to the change in the direction of the tangential stress, but also because of the repetitive change from tension to compression of the normal stress along the sliding direction. Therefore, the fatigue failure analysis is more appropriate and is conducted here by using the alternating von Mises stress, σ'_a, and mean von Mises stresses, σ'_m, given below:

$$\sigma'_a = \frac{1}{2^{1/2}}[(\sigma_{xa} - \sigma_{ya})^2 + (\sigma_{ya} - \sigma_{za})^2 + (\sigma_{za} - \sigma_{xa})^2 + 6\tau_{xza}^2]^{1/2} \tag{13}$$

$$\sigma'_m = \frac{1}{2^{1/2}}[(\sigma_{xm} - \sigma_{ym})^2 + (\sigma_{ym} - \sigma_{zm})^2 + (\sigma_{zm} - \sigma_{xm})^2 + 6\tau_{xzm}^2]^{1/2} \tag{14}$$

Alternating values (subscript a) and mean values (subscript m) of normal and shear stresses can be calculated using the following equations:

$$\sigma_{ka} = \frac{(\sigma_k)_{max} - (\sigma_k)_{min}}{2} \tag{15}$$

$$\sigma_{km} = \frac{(\sigma_k)_{max} + (\sigma_k)_{min}}{2} \tag{16}$$

To avoid repeating similar equations for each stress, the index k is introduced and could be replaced by x, y, z or xz for the case of the shear (σ becomes τ). The subscripts max and min represent the maximum and minimum amplitudes of the stress variations.

The following equation (known as the Marin equation) together with the Soderberg fatigue failure theory [9] are used here to predict fatigue failure, by evaluating the fatigue factor of safety, n:

$$\left(\frac{nK_1\sigma'_a}{S_e}\right)^m + \left(\frac{nK_2\sigma'_m}{S_u}\right)^p = 1 \tag{17}$$

where S_e and S_u are the endurance and ultimate strengths of the material and, for the Soderberg theory, $K_1 = m = p = 1$ and $K_2 = S_u/S_y$, S_y being the yield strength. The values of S_u and S_y used in this analysis are those given in Table I. It is well known that the plastics considered in this study do not have a specific endurance limit as defined for metallic materials; therefore, S_e is assumed to be equivalent fatigue strength at 10^6 cycles and was approximately evaluated as $S_u/3$, as recommended by some references. However, this might seem to be a too conservative approach since the design guides published by DuPont for Zytel 101 and Delrin 500 show that the fatigue strengths at 10^6 cycles for both materials is about $0.4S_u$.

4. Results and discussion

4.1. Coefficient of friction

Fig. 2 shows typical profiles of imposed constant normal load and sliding speed, v, as well as the corresponding dynamic response of the tribological system. This response is represented here by the frictional force acting at the contacting interface between the specimen and slider during the reciprocating motion. A constant stroke of 100 mm, which includes the overlaps at both ends, was selected and used for all friction tests. As can be seen from this figure, fluctuations in the frictional force occur during sliding with noticeable peaks arising at the start of each stroke, where the speed goes through zero during a very brief period of time yielding conditions of a transition from static to dynamic friction. Of particular interest to this study was the region of dynamic friction where very small fluctuations occur; therefore the so-called boundary effects were not considered in the evaluation of the coefficient of friction, μ. This parameter was evaluated from the ratio of frictional force to normal load, both simultaneously recorded at high sampling frequency by a data acquisition system. The values of μ reported here and later used in the contact stress calculations

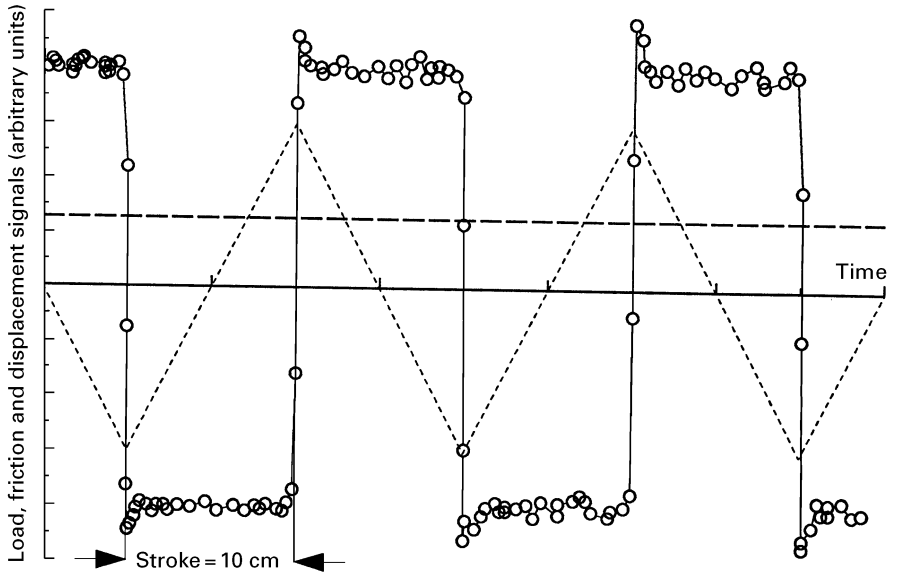

Figure 2 Time dependence of normal load (– –), displacement (– – – –) and frictional force (— ○ —) during reciprocating sliding friction testing.

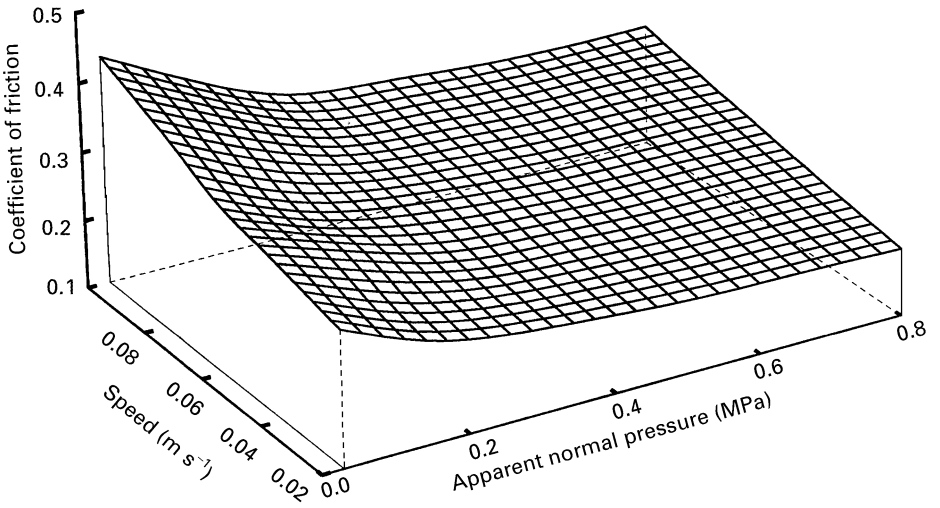

Figure 3 Initial dynamic coefficient of friction as a function of apparent pressure and speed for UHMWPE.

are average values of data obtained from six consecutive strokes (three in each direction of motion) after 20 cycles (1 cycle is equivalent to two strokes) of friction at constant testing conditions (speed and load) using between three and five different samples. Ranges of normal load varying between 5 and 160 N, and sliding speed between 0.01 and 0.1 m s^{-1} were utilized. These results are depicted, for the three materials, in Figs 3, 4 and 5 as three-dimensional graphs representing the variation in μ with sliding speed, v, and apparent normal pressure, P, which represents the ratio of applied normal load to apparent area of contact of the sample (200 mm^2).

Clearly, compared with UHMWPE and POM, distinct behaviour can be noted for PA 66 in a sense that it shows an increase in μ with increasing P, when the opposite is observed for the remaining plastics. At the same time the increase in μ with increasing v applies to all three materials. The same trend of data and order of magnitude were reported by many previous workers, who have on many occasions explained these behaviours. Moreover, a literature review showed that, unlike the most common thermoplastics, the friction of nylons is sensitive to the magnitude of normal load. Watanabe *et al.* [10] have reported an increase in μ with increasing P for this family of plastics at a range of moderate loads comparable with those of the present investigation and speed of 0.1 m s^{-1}, when sliding on steel in a thrust–washer arrangement.

4.2. Contact and subsurface stress evaluation

The following results are based on average values of the properties of the steel contacting surface. Young's modulus of 200 GPa and Poisson's ratio of 0.3 were used in all stress calculations. For the plastic materials, as indicated earlier, appropriate data were taken from Table I. Also, to limit the scope of this study, a fine roughness which is more often encountered in practical situations was selected and investigated

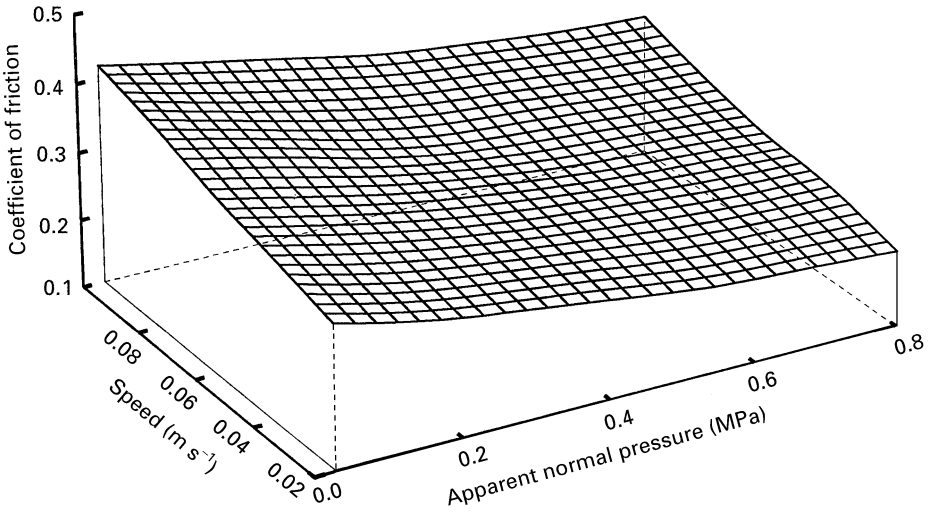

Figure 4 Initial dynamic coefficient of friction as a function of apparent pressure and speed for POM.

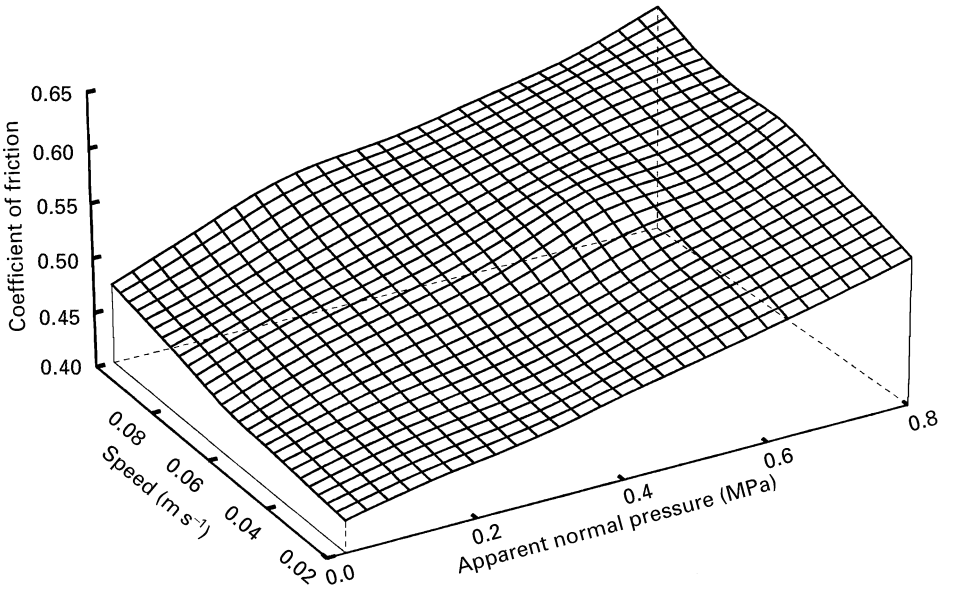

Figure 5 Initial dynamic coefficient of friction as a function of apparent pressure and speed for PA 66.

throughout the following analysis. It is worth emphasizing that the measured properties of the materials and coefficients of friction corresponding to each load for various sliding speeds were used in the present investigation, unlike previous general studies on contact stresses whose results are based on normalized parameters and assumed values of the coefficient of friction which may not accurately represent the conditions that define the actual tribological system.

An example of the variation in the stress tensor at each point of the contact region of each asperity along the x axis ($z = 0$; $y = 0$), is shown in Fig. 6, for UHMWPE selected as an example using the coordinate system shown in Fig. 1, as obtained from the closed-form solutions (Equations 2–5). The conditions relevant to these results are mentioned on the figure, which shows also the width, $2b$, of the rectangular contact zone and direction of sliding. As expected, tensile peaks for σ_x and σ_y arise at the trailing edge of the contact region with respect to the direction of friction. We should point out at this stage that the peak values of these tensile stresses were accurately calculated at the location corresponding to $x = -b$, the half-length of the contact, b, being precisely evaluated. The corresponding principal stresses as well as the maximum shear which is equal to $(\sigma_2 - \sigma_1)/2$ in the present case, and the von Mises stress (Equation 12) were evaluated and plotted in Fig. 7. According to these results, including those obtained for the remaining conditions and materials, τ_{max} and S_{vM} remain almost constant along the x axis. Also the amplitude of S_{vM} is very close to the peak tensile value of the principal stress, σ_2. Furthermore, as shown in Figs 8 and 9 (taken as examples), there is a noticeable variation in these two stresses along the z axis that represents the depth below the contact surface. In the case of UHMWPE and POM an increase with increasing z may occur, reaching a maximum value, but for PA 66 a decrease was always observed. It is apparent from these results that, when there is an increase, the

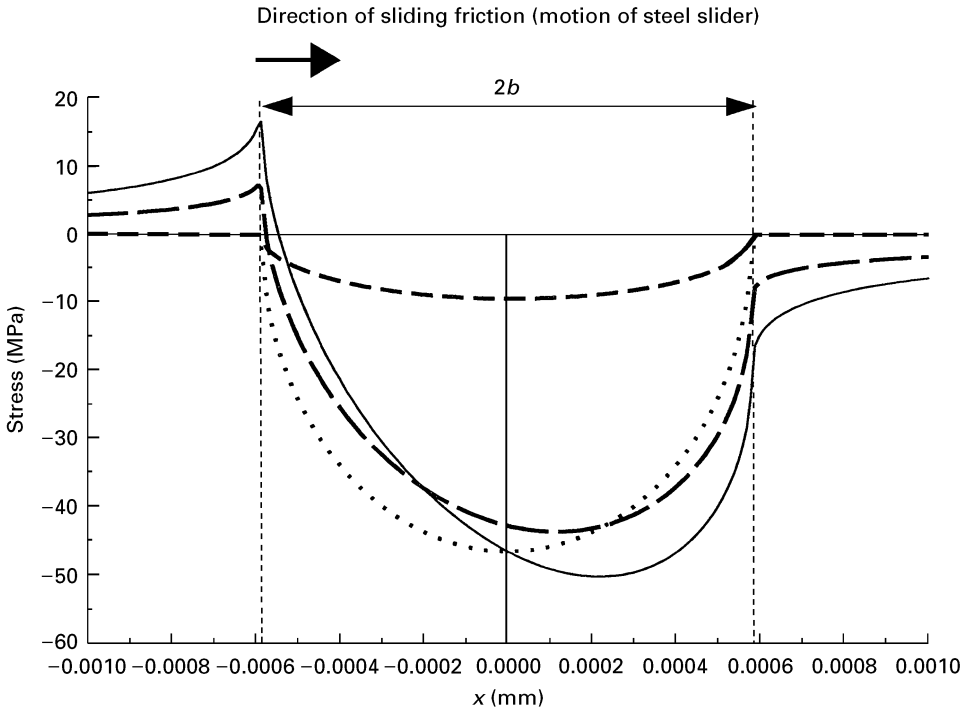

Figure 6 Variation in the stress tensor along the direction of sliding for UHMWPE ($\mu = 0.2$; $P = 0.8$ MPa; $v = 0.01$ m s^{-1}). (———), σ_x; (— — —), σ_y; (– – – – – –), σ_z; (– – –), τ_{xz}.

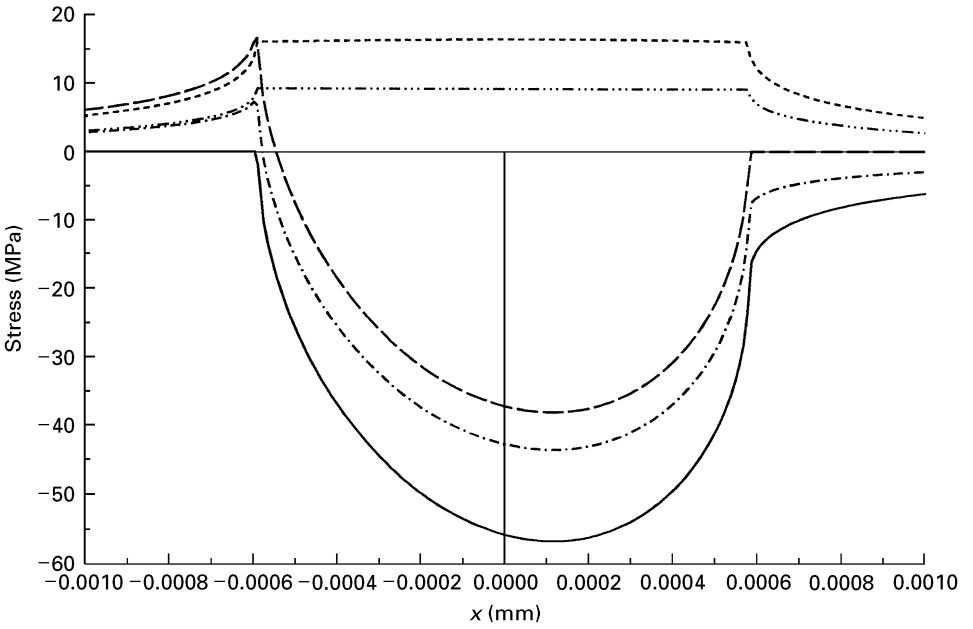

Figure 7 Variations in the principal stresses, σ_1 (——), σ_2 (— —) and σ_3 (—·—), maximum shear stress, τ_{max} (— ··· —), and von Mises stress, S_{vM} (– – – – – –) along the sliding direction for the same conditions as Fig. 7.

location (along z) at which the maximum value is registered is shifted towards deeper depths with increase in the load (corresponding to a decrease in the coefficient of friction in the cases of UHMWPE and POM) independently of sliding speed. On the other hand, the decrease in sliding speed tends to increase the magnitude of the difference between the value of this stress calculated at the contact zone ($z = 0$) and its corresponding maximum amplitude. The maximum values of S_{vM} (independently of the location at which they occur) are plotted, for the three materials, in Figs 10, 11 and 12 as a function of the coefficient of friction and the shown trend of the considered sliding speeds. These results show an increase in S_{vM} with decrease in μ in the cases of UHMWPE and POM, but the opposite observation is valid for PA 66. Also, for each speed, this variation can be relatively well approximated by a linear relationship shown by the solid lines in these figures. Similar behaviours were observed in the case of τ_{max}. Furthermore, these results

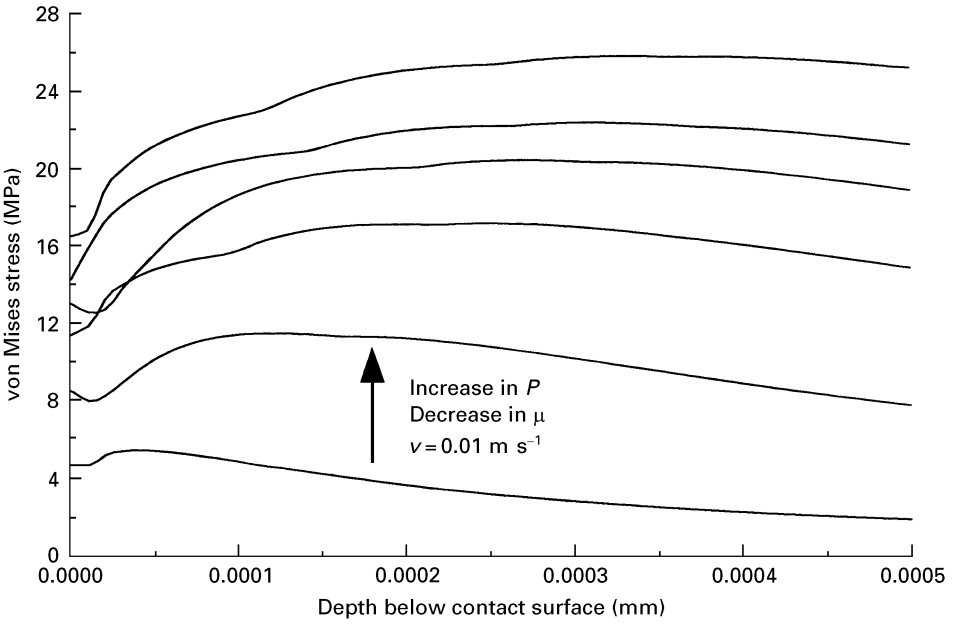

Figure 8 Variation in the von Mises stress with the depth for different contact pressures.

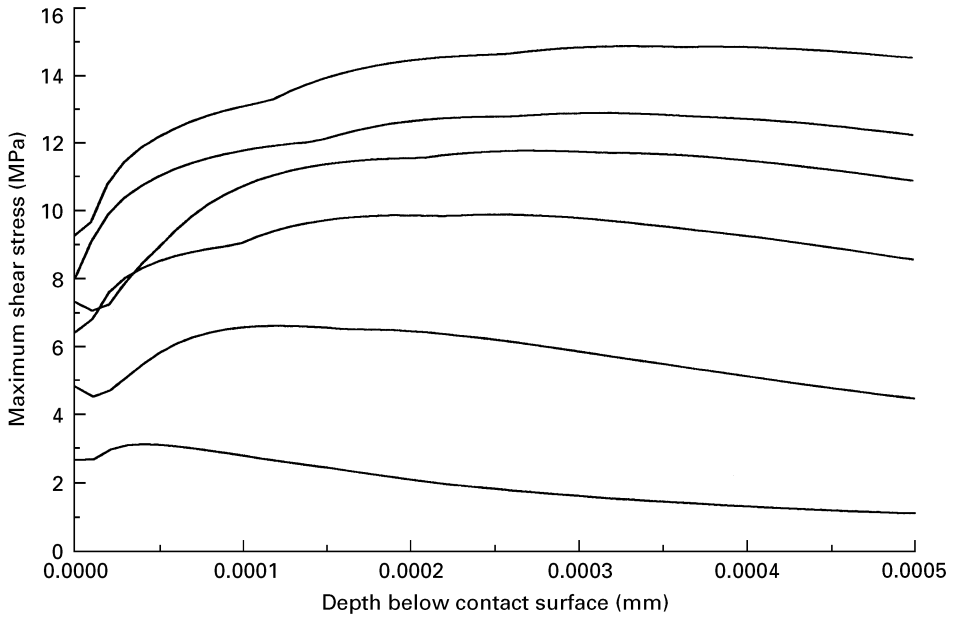

Figure 9 Variation in maximum shear stress with the depth for different contact pressures.

demonstrate a predominant effect of the load and therefore the decrease in the coefficient of friction with increasing load, which characterizes the first two materials, should not be interpreted as a decrease in contact stresses. Also, in the case of UHMWPE, S_{vM} and τ_{max} reach values higher than the yield and shear strengths (see Table I), at a relatively low apparent contact pressure $P = 0.8$ MPa, which indicates that inelastic behaviours take place. The relationship between the coefficient of friction and the depth below the contact surface, at which the maximum values of these two stresses occur was also investigated and the results are depicted in Figs 13 and 14, in which different sets of symbols are used to identify the different sliding speeds. These data demonstrate that this location shifts towards the contacting surface with increase in μ and reaches it when $\mu \approx 0.35$ for UHMWPE and $\mu \approx 0.32$ for POM.

It is important to mention once more that the present study deals with sliding friction in reciprocating motion. Under these conditions, a transition in the nature of the stresses, σ_x and σ_y, varying from tension to compression, takes place at the onset of each change in sliding direction. The combined loading introduced in this way and occurring at the edges of the contact zone ($x = \pm b$) initiates a fatigue

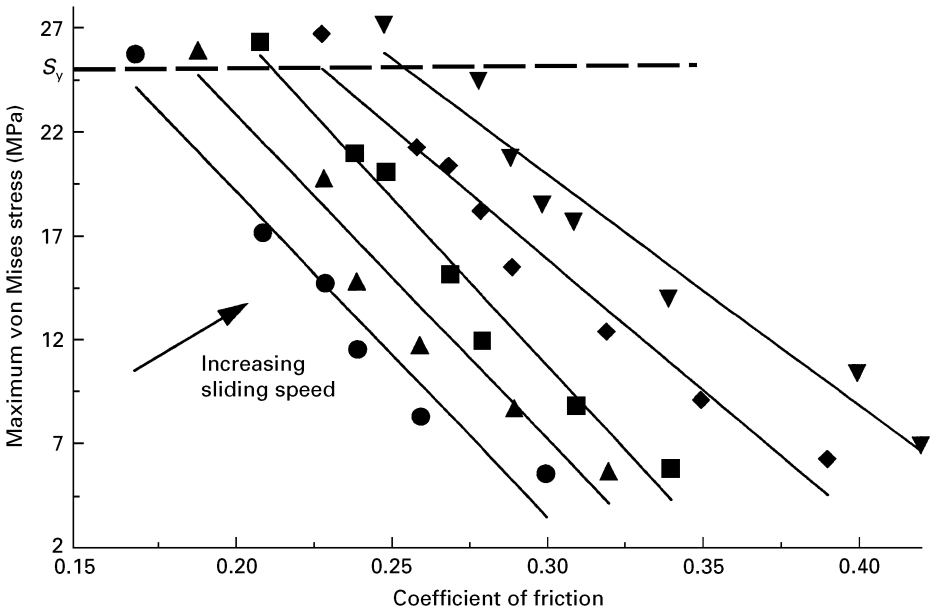

Figure 10 The maximum von Mises stress as a function of the coefficient of friction for different sliding speeds in the case of UHMWPE.

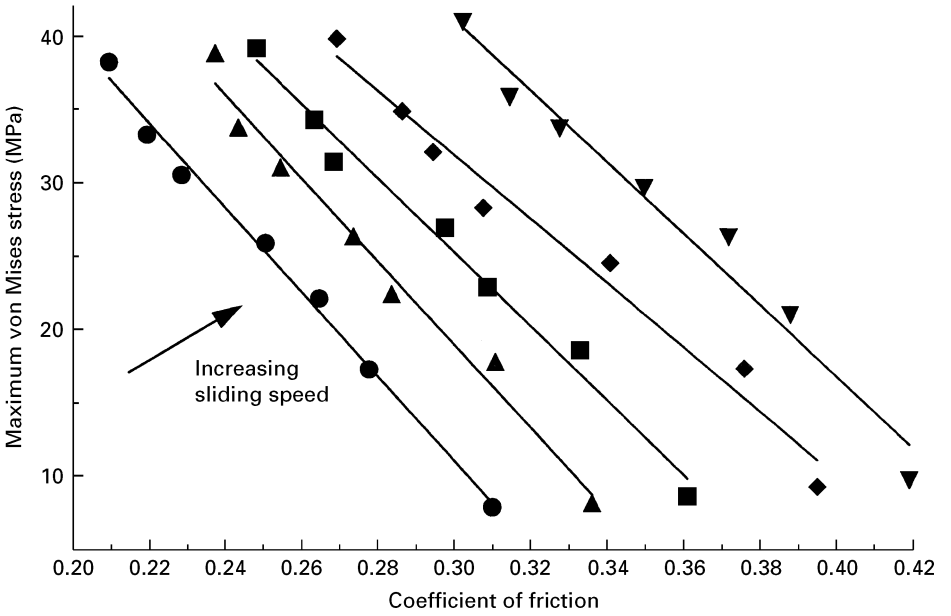

Figure 11 The maximum von Mises stress as function of the coefficient of friction for different sliding speeds in the case of POM.

phenomenon. The compressive fluctuation of these two stresses occurring inside the contact region was not considered. Also, it can be seen from the plots in Fig. 6 that σ_z is not affected by the reciprocating motion, as it remains constant, but a change in the sign of the shear stress τ_{xz} would result from the reciprocating motion. At the same time, it can be seen from the same figure that this stress tends to zero at locations where $x = \pm b$. Subsequent to these observations, it was deduced that the edges of the contact represent the critical locations where the considered fatigue failure might be initiated. Therefore, the alternating and mean values of the stresses (based on Equations 15 and 16) used in the determination of the alternating and mean von Mises stresses given by Equations 13 and 14 were evaluated considering the following conditions: $(\sigma_x)_{max} = (\sigma_x \text{ at } x = -b)$ and $(\sigma_x)_{min} = (\sigma_x \text{ at } x = b)$, the same reasoning applying to σ_y, and at the same time $\sigma_{z\,a} = \sigma_{z\,m} = 0$ and $\tau_{xz\,a} = \tau_{xz\,m} = 0$. Moreover, it was decided to refer to the frequency rather than the sliding speed in the following analysis, because of its relevance to dynamic situations where fatigue becomes an important factor. This parameter was defined here as the ratio of sliding speed and stroke (equal to 0.1 m). Fig. 15 shows an example of the variations in σ'_a and σ'_m as functions of

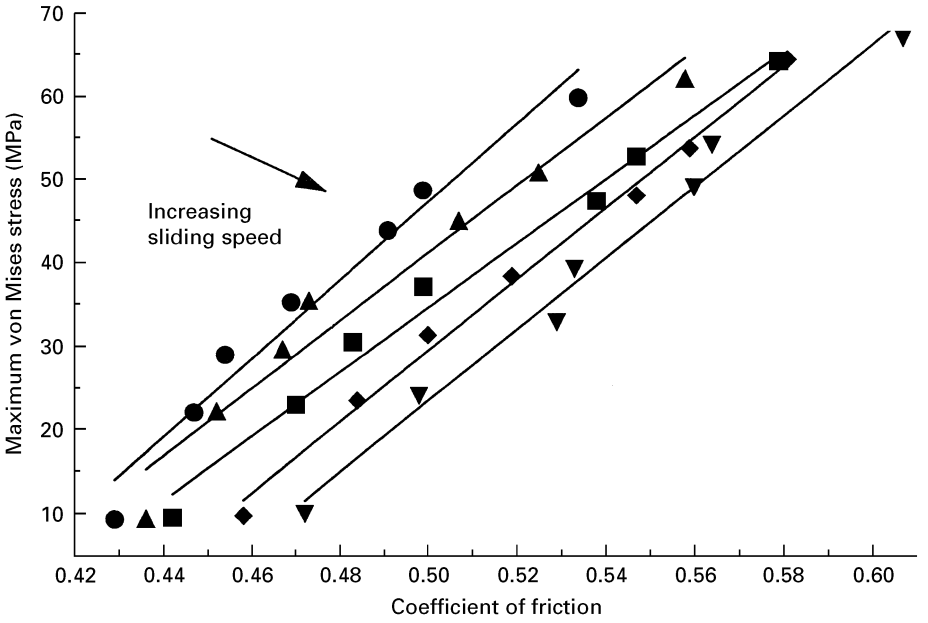

Figure 12 The maximum von Mises stress as function of the coefficient of friction for different sliding speeds in the case of PA 66.

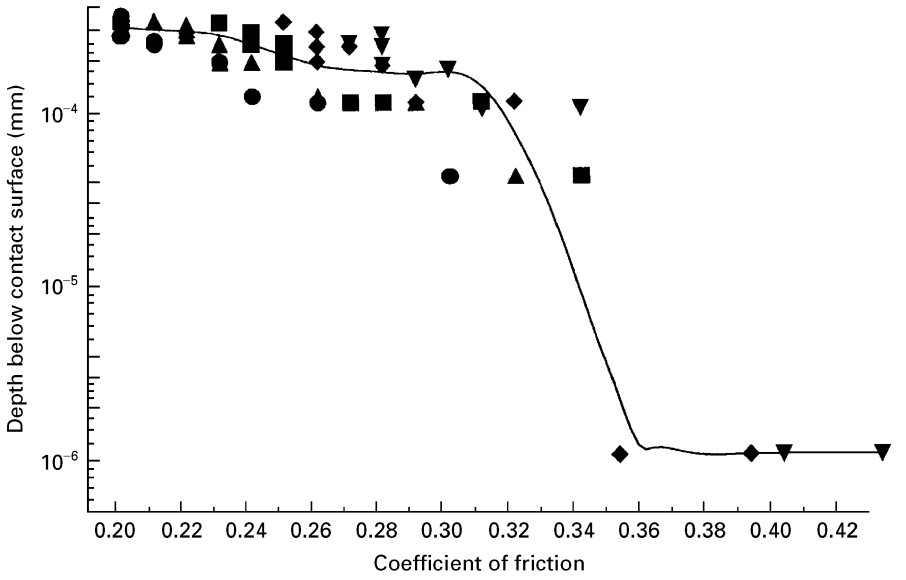

Figure 13 Locations of points at which maximum values of the von Mises stress occur in the case of UHMWPE.

the depth z. This particular fatigue failure analysis, which focuses on locations where the shear does not act, has produced a difference between the behaviours of the two stresses, so that their respective maximum values (always higher in the case of σ'_a) occur at different locations: at contact surface ($z = 0$) for the alternating value and below it ($z \neq 0$) for the mean value, independently of the tested experimental conditions and materials. As a simplified approach, these results were further used in the determination of the factor of safety, n, using Equation 17. Because of the above-mentioned pronounced difference between the behaviours of the two pertinent stresses, it was felt appropriate to evaluate n for the conditions pertaining to each of the two locations where the variation in each stress passes through its maximum. It was found that the contacting surface ($z = 0$) was the most critical in the sense that it was there where the minimum value of n was obtained. Fig. 16 summarizes the results of this fatigue analysis for the case of POM taken as example. This three-dimensional graph shows the variation in n as a function of P and frequency. It appears that n decreases with increase in these two parameters, reaching critical situations at conditions identified by symbols on the graph. To permit easy use of the present results during the design of practical applications involving reciprocating friction of the present materials, the limiting value $n = 1$ was selected

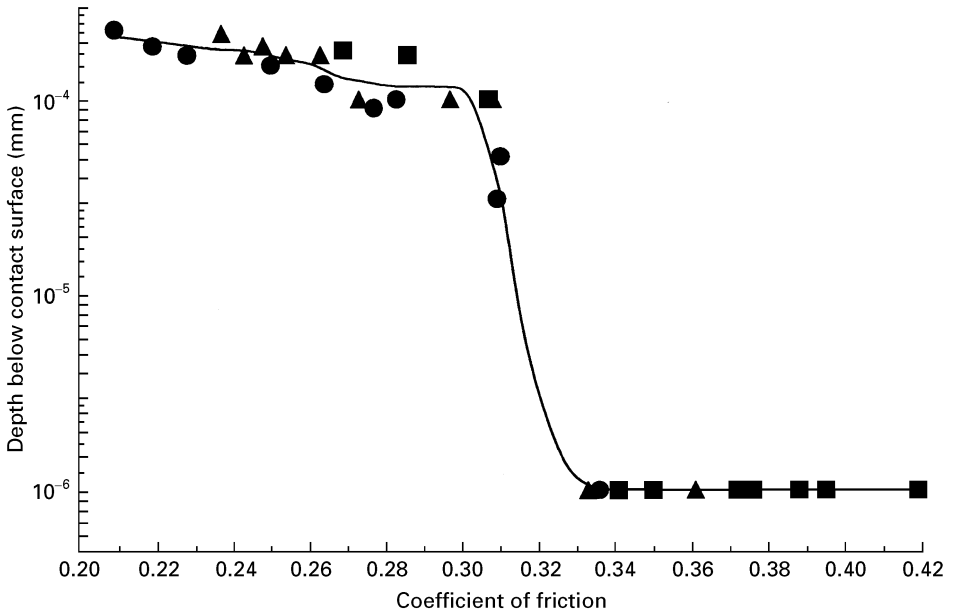

Figure 14 Locations of points at which maximum values of the von Mises stress occur in the case of POM.

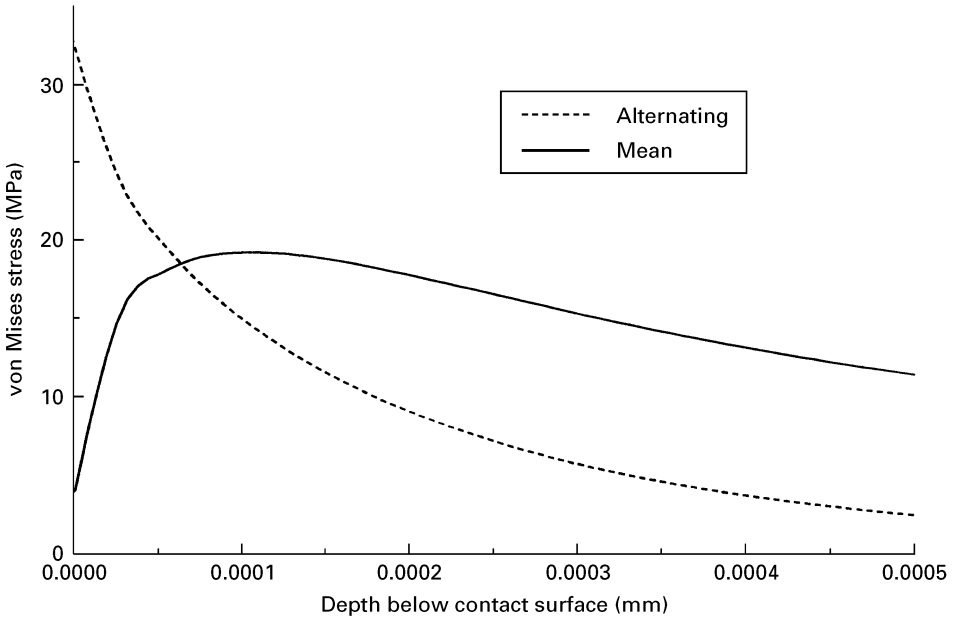

Figure 15 Variations in the alternating (– – – – – –) and mean (——) von Mises stresses with the depth below the contact surface.

as criterion for fatigue failure which might be an important factor in formation and propagation of cracks leading to excessive wear. The results of this investigation permitted the construction of Fig. 17 showing the transition, expressed as load and frequency capability factors of each material, that marks the onset of wear mechanism arising from fatigue failure. The same figure may be interpreted as a way of ranking these materials with respect to their wear performance at the conditions of the present study, suggesting advantageous use of POM followed by PA 66 and then UHMWPE. It is interesting to note that wear results of many polymers (among them POM and PA 66), although obtained under different experimental conditions from those of the present study by Mens and Gee [11], confirm that only POM is suitable for use under dry running against steel. On the other hand, results reported by Anderson [12] support the previous conclusion but show a specific wear rate of UHMWPE lower than that of POM, when derived from thrust bearing tests with a bearing pressure of 1 MPa and sliding speed of $0.03\,m\,s^{-1}$ against mild steel. The present research continues in carrying out wear testing under the present conditions. This will certainly enable us to assess accurately the relationship between the reported fatigue failure and wear rate and to draw conclusions about the impact of the reciprocating motion on the wear process.

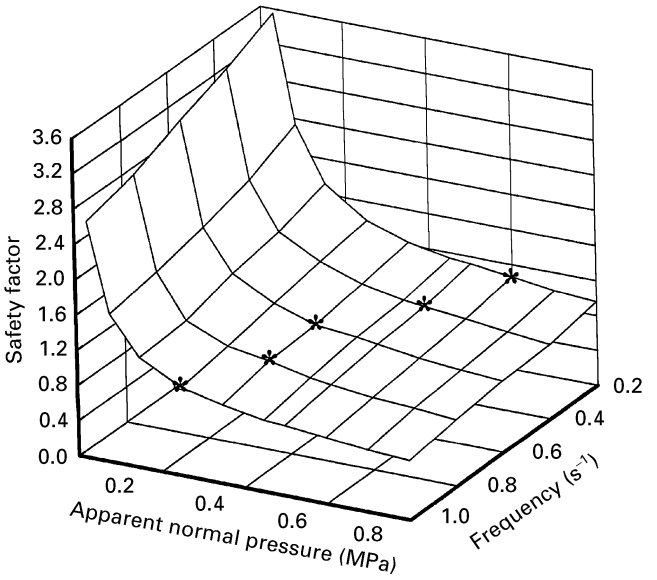

Figure 16 Safety factor as a function of frequency of reciprocating motion and apparent contact pressure.

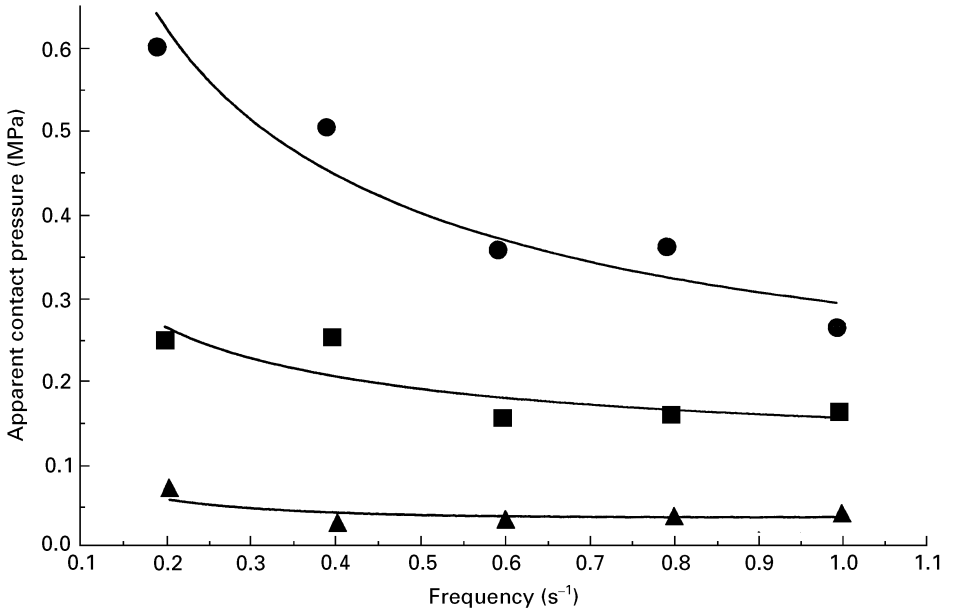

Figure 17 Contact pressure and frequency limits for UHMWPE (▲), POM (●) and PA 66 (■).

4.3. Scanning electron microscopy observations

The results from the above analysis indicate that the relatively mild conditions considered in our work were sufficient to develop large contact stresses during friction. The main objectives of the following part of the paper, which is based on the results from morphological observations of worn contact surfaces, constitute an attempt to understand further and to illustrate the mechanism of formation of wear particles at the conditions that define the present tribological system. A scanning electron micrograph of the rubbing surface after 100 cycles (equivalent to a travelled distance of 20 m) is shown in Fig. 18. It appears that rectangular areas are formed at the tips of asperities and at the same time, compressive stresses induce

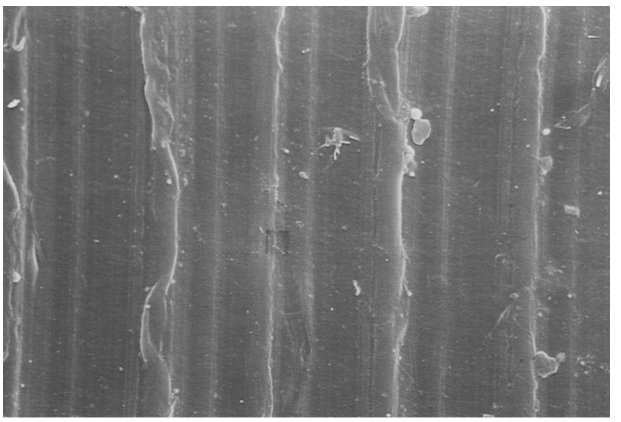

Figure 18 Scanning electron micrograph of initial transformations of the contacting surface at 585× for UHMWPE ($P = 0.8$ MPa; $v = 0.1$ m s^{-1}).

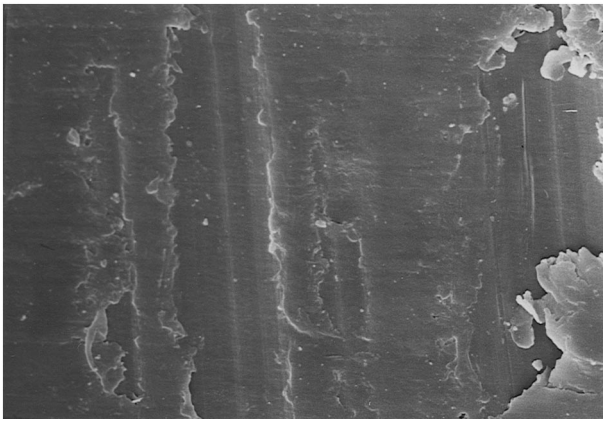

Figure 19 Scanning electron micrograph of development of transfer film at 585× for UHMWPE ($P = 0.8$ MPa; $v = 0.1$ m s^{-1}).

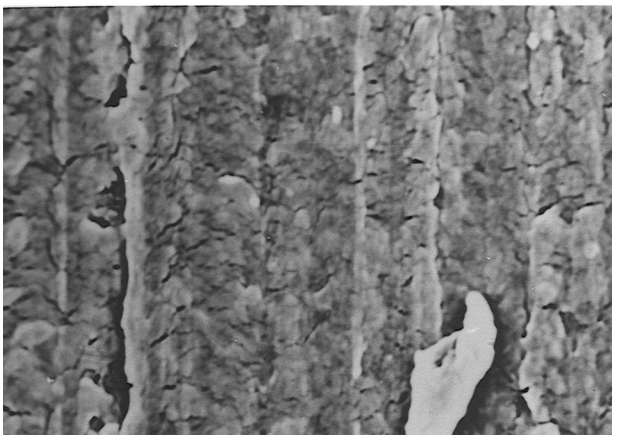

Figure 20 Scanning electron micrograph of establishment of the transfer film at 700× for UHMWPE (same conditions as Fig. 19).

a "spread" of material in the form of a film away from asperities, to regions where actual contact did not occur. As a consequence, wear debris formation is very evident and seem to result from the fracture of some edges of the "free" extremities of this layer-like material. Finer debris might be caused by the very light abrasion process that takes place in the early stages of friction. After 500 cycles (100 m), as can be seen in Fig. 19, film patches continue to grow by spreading until the whole surface is covered by a physical interface best known as a third body. From these two observations, it seems evident that critical regions are developed where these individual patches meet during the procedure of gradual formation of the transfer film. A welding process or roll-over mechanism may take place at these junctions, leading to physical boundaries having distinct properties. These micrographs show clearly that no tearing occurs, which is a strong indication that any abrasive phenomenon was probably negligible, thus validating the assumption of combination of adhesive and fatigue mechanisms on which the contact stress analysis was based. On the other hand, the combination of high contact stresses and heat generated during sliding contribute certainly to yield morphological properties of this layer-like material that are different from those of the initial contacting surface. It was already established by previous researchers, among them [13], that a preferential orientation of molecular chains is developed, but we can add that the severe work-hardening process that takes place in the film affects its degree of crystallinity and energy of adhesion. It is clear that these modifications of the tribological system have an impact on its frictional behaviours. Also, the first two micrographs (Figs 18 and 19) demonstrate that, after sliding for just a few cycles (short sliding distance), drastic changes in the initial roughness and area of contact resulted. This observation concurs with the results obtained from the fatigue failure analysis, showing relatively low values of the safety factor, which indicates high probability of fatigue wear. Therefore these two interrelated parameters, namely the number of cycles and the safety factor, should play an important role in the wear rate generated during

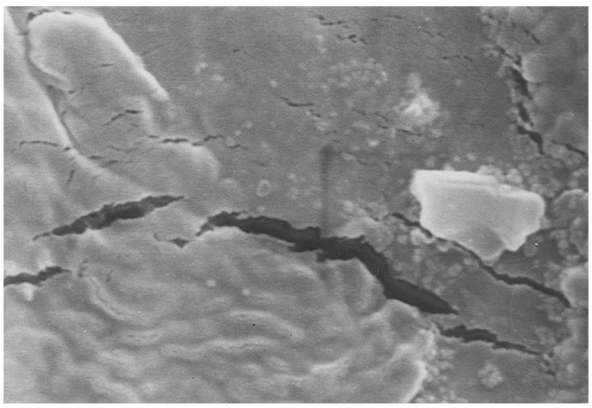

Figure 21 Scanning electron micrograph of cracks and wear debris at 7700×.

the present type of friction. Subsequently, as depicted in Fig. 20, the contacting surface of the plastic material becomes completely covered by an irregular film weakened by a large number of cracks that are more evident in the micrograph in Fig. 21, taken at a high magnification, which shows not only the cracked layer but also subsurface cracks. It is interesting to note that, although the predominant orientation of these flaws is close to normal to the direction of sliding represented by the arrow in the figure, others are oriented along this direction. The latter were most probably created by the contact stress developed along the y axis. At the same time, this figure emphasizes once more the distinct wear phenomena of layer formation and wear particles reported earlier. It seems that the wear particle formation occurs in two different stages: an early stage as introduced above and responsible for the formation of small particles, and the second stage due to the roll formation initiated by a tearing-off of the layer which produces platelets as fracture occurs at its weak regions, followed by a roll-over and a rolling process of these particles out of the contact region as shown in Fig. 22. This behaviour, which is certainly accentuated by the reciprocating motion, has led to a very apparent accumulation of the plastic material in the form of powder debris at

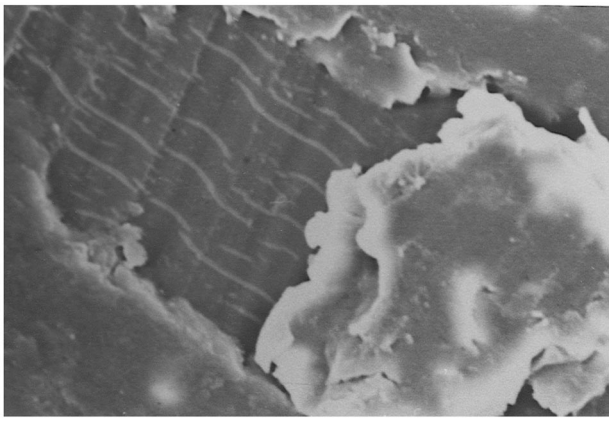

Figure 22 Scanning electron micrograph of roll formation at 700 × forUHMWPE.

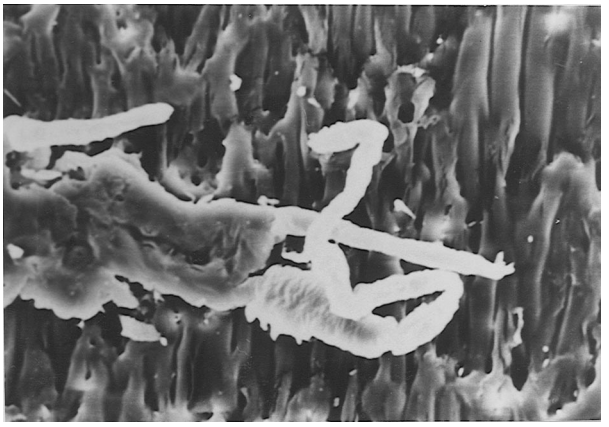

Figure 23 Scanning electron micrograph of roll formation at 690 × for PA 66.

regions of the slider corresponding to stroke ends. Despite the presence of some wear particles transferred to the metallic surface (slider), there was no direct evidence of adhesion of the film to the slider, which was rather attached to the surface of the plastic material during friction in the case of the conditions of the present study. Roll formation was observed to be the main mechanism of formation of wear debris after the establishment of the transfer film, for the three thermoplastics. The micrographs in Fig. 22 above and in Fig. 23 support this statement.

In parallel with the scanning electron microscopy (SEM) observations, it was evident from qualitative evaluations of the amount of wear that the contact pressure was the principal factor that affects this parameter, agreeing with the previous result from the stress analysis and suggesting an increase in the critical contact stresses with increase in the normal load despite the decrease in the coefficient of friction that takes place at the same time for most thermoplastics. This leads us to believe that a reduction in the normal load, creating conditions of higher factors of safety, would be beneficial for wear reduction due to fatigue. Note that we have voluntarily referred to the normal load to avoid the confusion arising from the decrease in the contact pressure with the progression of wear process which leads to an obvious increase of the real area of contact. Also, the results of the present study gave a strong indication that the proposed fatigue analysis could be used with reasonable confidence to assess the importance of the fatigue component in similar tribological systems.

5. Conclusion

Experiments were conducted to measure accurately the dynamic coefficient of friction of three engineering thermoplastics: UHMWPE, POM and PA 66. Reciprocating sliding friction and plane-on-plane dry contact with a polished steel slider were the most important parameters that define the tribological system studied. A brief analysis of the influence of the normal load and speed on the coefficient of friction showed in general similar relationship to those found by many researchers in the case of continuous motion.

The application of elastic non-Hertzian stress analysis to a simplified model consisting of cylindrical tips of asperities of the plastic material making contact with a smooth and hard semi-infinite plane was performed in this investigation. The measured coefficient of friction μ and mechanical properties of the plastic materials, together with topographical parameters derived from the surface roughness profile, were used in the calculation of contact stresses.

Two of the principal stresses are changed into tensile stresses at the trailing region of the frictional force, and the von Mises stress as well as the maximum shear stress remain almost constant along the sliding direction, but their respective maximum values occurs at different depths depending on the material and μ. For PA 66 this location is located always at the contact surface, but for the remaining materials the subsurface location moves towards the interface with increase in μ, reaching it when μ is equal to about 0.35 for UHMWPE and about 0.32 for POM.

The relationship between the maximum values of S_{vM} and τ_{max} and the value of μ, for each sliding speed, can be well approximated by linear relationships which show an increase in these values with decrease in μ. Therefore the normal loading has a more predominant effect on the contact stresses than μ.

The application of the fatigue failure criterion based on the combination of the Marin equation and the Soderberg theory at the critical point, which in this case was the edge of the area of contact of each asperity, permitted us to determine the limits of application of each material expressed as apparent contact pressure and frequency that mark the onset of crack formation leading to excessive fatigue wear. According to these results, POM is the only material that shows reasonable limits for practical applications, ranging from 0.3 MPa at a high frequency (1 Hz) and reaching higher pressures (limited probably by the yield strength) at frequencies below 0.2 Hz. These results can easily be extended to cover a larger range of conditions and materials by considering a well-defined model to which the proposed fatigue failure analysis might be applied to derive similar graphs to those shown in Fig. 17. This graphical representation could be used as an easy tool for a quick selection of optimal

tribological parameters that avoid excessive fatigue wear in practical applications.

SEM observations of the worn surface of the plastic materials showed evidence of the development of cracks due to fatigue and also permitted us to conclude that roll formation is in the present case the principal mechanism of formation of wear particles after the establishment of the transfer film.

Qualitative evaluations of the amount of wear demonstrate that the normal load is the most critical parameter that affects the fatigue wear and its reduction would certainly produce beneficial effects.

References

1. S. WU, "Polymer interface and adhesion" (Marcel Dekker, New York, 1981).
2. D. DAWSON, M. M. EL-HADI DIAB, B. J. GILLIS and J. R. ATKINSON, "Polymer wear and its control", edited by L. H. Lee (American Chemical Society, Washington, DC, 1985) pp. 171–187.
3. K. TANAKA and T. NAGAI, "Wear of materials", edited by K. C. Ludema (American Society for Mechanical Engineers, New York, 1985) pp. 253–298.
4. D. M. TOLSTOI, *Wear* **10** (1967) 193.
5. H. BENABDALLAH and J.-P. CHALIFOUX, *Tribol. Int.* **24** (1991) 403.
6. I. V. KRAGELSKI and V. V. ALISIN, "Friction, wear and lubrication", Vol. 1 (Pergamon, Oxford, 1981).
7. S. H. BENABDALLAH and J.-P. CHALIFOUX, *Tribol. Int.* **22** (1989) 383.
8. A. P. BORESI and O. M. SIDEBOTTOM, "Advanced mechanics of materials" (Wiley, New York, 1985).
9. J. S. E. SHIGLEY, "Mechanical engineering design" (McGraw-Hill, New York, 1988).
10. M. WATANABE, M. KARASAWA and K. MATSUBARA, *Wear* **12** (1968) 185.
11. J. W. M. MENS and A. W. J. GEE, in "Proceedings of the 8th International Conference on Wear of Materials", Vol. 1 (ASME, New York, 1991) pp. 563–570.
12. J. C. ANDERSON, in "Friction and wear of polymer composites," edited by K. Friedrich (Elsevier, Amsterdam, 1986) pp. 329–362.
13. J. L. KRZEMINSKY and E. WIECHOWWICZ-KOWALSKA, *Polym. Engng Sci.* **21** (1981) 594.

Received 30 July 1996
and accepted 10 February 1997